# Three-Dimensional Structure of the Neurotoxin ATX Ia From *Anemonia sulcata* in Aqueous Solution Determined by Nuclear Magnetic Resonance Spectroscopy

Hans Widmer, Martin Billeter, and Kurt Wüthrich
*Institut für Molekularbiologie und Biophysik, Eidgenössische Technische Hochschule-Hönggerberg, CH-8093 Zürich, Switzerland*

**ABSTRACT** With the aid of ^{1}H nuclear magnetic resonance (NMR) spectroscopy, the three-dimensional structure in aqueous solution was determined for ATX Ia, which is a 46 residue polypeptide neurotoxin of the sea anemone *Anemonia sulcata*. The input for the structure calculations consisted of 263 distance constraints from nuclear Overhauser effects (NOE) and 76 vicinal coupling constants. For the structure calculation several new or ammended programs were used in a revised strategy consisting of five successive computational steps. First, the program HABAS was used for a complete search of all backbone and $\chi^1$ conformations that are compatible with the intraresidual and sequential NMR constraints. Second, using the program DISMAN, we extended this approach to pentapeptides by extensive sampling of all conformations that are consistent with the local and medium-range NMR constraints. Both steps resulted in the definition of additional dihedral angle constraints and in stereospecific assignments for a number of β-methylene groups. In the next two steps DISMAN was used to obtain a group of eight conformers that contain no significant residual violations of the NMR constraints or van der Waals contacts. Finally, these structures were subjected to restrained energy refinement with a modified version of the molecular mechanics module of AMBER, which in addition to the energy force field includes potentials for the NOE distance constraints and the dihedral angle constraints. The average of the pairwise minimal RMS distances between the resulting refined conformers calculated for the well defined molecular core, which contains the backbone atoms of 35 residues and 20 interior side chains, is 1.5 ± 0.3 Å. This core is formed by a four-stranded β-sheet connected by two well-defined loops, and there is an additional flexible loop consisting of the eleven residues 8–18. The core of the protein is stabilized by three disulfide bridges, which are surrounded by hydrophobic residues and shielded on one side by hydrophilic residues.

## INTRODUCTION

ATX Ia is one of a series of polypeptide toxins used by the sea anemone *Anemonia sulcata* to paralyze its prey of crustaceans and small fishes.[1,2] These small proteins exert strong effects on the mammalian heart and on mammalian and crustacean nerves, apparently by slowing down the inactivation of the sodium channel by extending the period of the inward sodium current. Sea anemone toxins share this presynaptic action with scorpion toxins, whereas α and β neurotoxins from snakes interact with the synaptic or postsynaptic membranes.[2] The electrophysiological effects of sea anemone toxins have been subject of intensive studies, but the data thus accrued have not as yet been matched by information on the three-dimensional structure of this class of compounds. The present paper describes the determination of the solution conformation of ATX Ia by nuclear magnetic resonance spectroscopy (NMR).

There are no crystal structures available as yet, but several sea anemone toxins that are homologous to ATX Ia are currently investigated by NMR in order to determine the three-dimensional structure in solution. Sequence-specific NMR assignments have been reported for a preparation of ATX I from *Anemonia sulcata*,[3] ATX Ia from *Anemonia sulcata*,[4] AP-A from *Anthopleura xanthogrammica*,[5] RP II[6] and RP III[7] from *Radianthus paumotensis*, and Neurotoxin I from *Stichodactyla helianthus*.[8]

Based on the resonance assignments, the secondary polypeptide structures were determined with variable degrees of completeness, for AP-A a description of the three-dimensional backbone fold was presented,[9] and for RP II a three-dimensional structure is also available (D. Wemmer, private communication). All the proteins studied consist of 46–49 residues. They show a large degree of sequential homology, including the conserved locations of six cysteines.[7] For ATX II, which is another homologous toxin from *Anemonia sulcata,* the three disulfide bridges were determined with chemical methods.[10] For ATX Ia the disulfide locations were established by NMR,[4] and presumably the same disulfide combinations are conserved in the other sea anemone toxins. Just before this paper was submitted the three-dimensional structure of another related protein was presented, i.e., the 43 residue polypeptide BDS-I from *Anemonia sulcata.*[11,12] However, the relation of ATX Ia to this protein is less clearcut, since the sequence homology of BDS-I with the forementioned toxins is only about 30%, and its pharmacological properties are different from those of the toxins.

ATX I is a mixture of two isoproteins, ATX Ia and ATX Ib, which differ in only one sequence position: Ala 3 of ATX Ia is replaced by Pro in ATX Ib.[13] Previously, with the aid of the complete sequential assignments of ATX Ia and a preliminary analysis of NOE distance constraints, scalar couplings $^3J_{HN\alpha}$, and exchange rates of the amide protons, a schematic representation of a four-stranded β-sheet could be derived.[4] The present calculation of the complete three-dimensional structure uses new procedures to extract unambiguous local conformational information from intraresidual, sequential and medium-range NMR constraints. The underlying principle is to use a complete search of the low-dimensional subspaces describing the local conformations of short polypeptide segments. These exhaustive searches guarantee that one finds *all* conformations that satisfy the local constraints. The results obtained were used to define additional conformational constraints to be added to the input for the structure determination, in particular also to obtain promising, but not inadequately biased starting structures. Compared to conventional distance geometry calculations,[14] superior reliability of the intermediate results obtained by this structural preprocessing is achieved, since the procedure does not depend on a small number of randomly generated starting conformations, and it is not limited by the relatively low convergence rate of the available optimization algorithms.

## EXPERIMENTAL PROCEDURES

A sample of ca. 10 mg of ATX Ia which was extracted from the venom of *Anemonia sulcata*[15] and repurified to separate it from the isoprotein ATX Ib[4]

was given to us by M. Lazdunski and H. Schweitz. In different experiments this material was used to prepare 0.5 ml of a ca. 0.004 M ATX Ia solution either in a mixture of 90% $H_2O$ and 10% $^2H_2O$ or, after exchange of all labile protons, in 99.98% $^2H_2O$. The pH was adjusted to 3.8 by addition of minute amounts of NaOH and HCl, or $NaO^2H$ and $^2HCl$, respectively.

The NMR data used as input for the structure determination were obtained from spectra recorded at 11°C on a Bruker WM 500 spectrometer. NOESY experiments[16] were recorded with mixing times of 200, 120, and 60 ms in $H_2O$, and 200, 100, and 50 ms in $^2H_2O$. ROESY spectra[17,18] were obtained using a spin lock consisting of a series of 30° pulses with a 30 kHz repetition rate,[19] with $\tau_m$ = 80 ms in $H_2O$, and 40 and 80 ms in $^2H_2O$. In all experiments the carrier was set in the center of the spectrum and quadrature detection was applied in both dimensions.[20] For the Fourier transformation of the time domain spectra, typically 1,024 and 512 data points in $t_2$ and $t_1$, respectively, were multiplied by a shifted sine bell window[21] and expanded by fourfold zero filling in both dimensions, which resulted in a digital resolution of 2.9 Hz/point in $\omega_2$ and 5.8 Hz/point in $\omega_1$. The base plane was corrected along $\omega_1$ by the method of Otting et al.[22] to eliminate $t_1$ ridges, and along $\omega_2$ by a polynominal fit to a set of predefined baseline points. The interpretation of the NOESY and ROESY spectra was based on the complete sequence-specific resonance assignments of ATX Ia at 11°C and pH 3.8.[4] Empirical distance calibrations of the sequential $d_{\alpha N}$ connectivities were based on the known range for this distance, i.e., $d_{\alpha N}^{min}$ = 2.2 Å in β-strands, and $d_{\alpha N}^{max}$ = 3.6 Å.[23,24] In the 60 ms NOESY spectrum in $H_2O$ most of the $d_{\alpha N}$ cross peaks of the polypeptide segments 2–6, 18–24, 31–34, and 41–46, which were previously shown to form β-strands,[4] had strong intensity. Nearly all other $d_{\alpha N}$ connectivities were also observed, but with generally weaker intensities. The few exceptions were due to the fact that some α proton resonances were bleached out by the preirradiation of the solvent signal, or to ambiguities arising from peak overlap. The weakest and strongest $d_{\alpha N}$ connectivities were used as references for the distance calibration, and on this basis the medium and strong $d_{\alpha N}$ cross peaks in the 60 ms NOESY spectrum in $H_2O$ were related to upper bounds of 2.8 Å and 2.4 Å, respectively. For the sequential distances $d_{NN}$ and $d_{\beta N}$, and the intraresidual connectivities observed in the spectra recorded with mixing times $\tau_m$ shorter than 80 ms, upper distance constraints of 4.0 Å, 3.0 Å, and 2.5 Å, respectively, were attributed to weak, medium and strong cross peaks, and only those constraints were included in the input for the structure calculation that represented a true constraint on the sterically accessible distance range.[23–25] For the longer-range distances upper bounds of 4.0 Å or 5.0 Å were used,

depending on whether the NOE's were observed with mixing times of $\leq 120$ ms, or only at 200 ms, respectively. Constraints with methyl groups or methylene protons that could not be stereospecifically assigned were referred to pseudo atom positions, and the appropriate corrections for the upper bounds were used.[25]

## COMPUTATIONAL PROCEDURES

The structure calculations included five steps. First, the local NOE distance constraints and the J-couplings were checked for internal consistency. To this end molecular fragments centered about each individual amino acid residue i and including the atoms $C=O^{i-1}$, $N\text{-}H^i$, $\alpha CH^i$, $\beta CH^i_n$, $C=O^i$, and $N\text{-}H^{i+1}$ were identified and subjected to a grid search of the entire conformation space spanned by the dihedral angles $\phi_i$, $\psi_i$, and $\chi^1_i$, using the program HABAS.[26] Each of the conformations thus generated was then checked for inconsistencies with the experimental constraints and the steric constraints. Internally inconsistent experimental data were identified when no conformation could be found that simultaneously satisfied all NMR constraints and the steric requirements. Once such inconsistencies were eliminated, HABAS further provided stereospecific assignments of the β-methylene protons for those residues where a sufficiently large number of sufficiently precise intraresidual and sequential NMR constraints were available to eliminate one of the two possible stereospecific assignments.[26] The stereospecific assignments thus obtained were then used to replace the pseudoatoms[25,27] by the individual β-methylene protons. Based on the thorough grid search, HABAS further identified those ranges of values for the dihedral angles $\phi$, $\psi$, and $\chi^1$ of each residue that are allowed relative to the local NMR constraints and the steric requirements.

A significant percentage of the total number of NOE distance constraints in proteins are medium-range constraints between residues separated by not more than 5 positions in the sequence.[27] This fact was exploited in the second step, where the variable target function program DISMAN[28] was run 500 times up to level 5, i.e., considering only interactions between residue pairs (i,j) with $|i-j| \leq 5$. In addition to the NOE distance constraints the input included the dihedral angle constraints determined with HABAS, the steric constraints, and a single medium-range hydrogen bond between residues 28 and 31. About 90% of the 500 resulting structures contained one or several significant constraint violations along the protein sequence. In contrast, each tripeptide segment converged locally in at least 100 out of the 500 structures. Because of this scarcity of global convergence at level 5, the following procedure had to be used to obtain statistically significant data. All 500 structures were scanned for residues i where

there was no residual constraint violation in any of the residues (i−1), i and (i+1) that would exceed 0.25 Å for NOE constraints and steric constraints, or 5° for dihedral angle constraints. From all structures in which a residue i satisfied these criteria, the distribution of the dihedral angle values for this residue was computed. The range of values covered was used to further supplement the input list, where it replaced the allowed range previously obtained from HABAS in all those cases where the latter range was less constrained. This procedure further provided a check for inconsistencies of the experimental constraints up to level 5, and new stereospecific assignments could be obtained based on the extensive sampling of usually several hundred structures for any given residue.

In a third step the program DISMAN[28] was applied to 100 starting conformations with input lists that had been updated using the stereospecific assignments and the new dihedral angle constraints obtained in the first two steps. The previously identified hydrogen bonds[4] and the three disulfide bonds were also added, using the standard distance constraints.[27,29] The starting conformations were randomly chosen within the regions of local conformation space defined by the forementioned dihedral angle constraints. During the calculations those among the 100 runs were stopped and discarded that did not meet specified convergence requirements at intermediate levels. Forty runs were computed up to the final level 46, where all experimental and steric constraints were considered. The resulting conformers were then ranked according to the sum of the residual violations of constraints. Thereby a significant reduction in the quality was observed between the conformers 8 and 9. For example, the maximum violation of any steric constraint was $\leq 0.5$ Å in the first eight DISMAN solutions, and it amounted to 0.9 Å in solution 9. Therefore only the best eight conformers were subjected to further refinement and subsequently used for the description of the solution structure of ATX Ia.

In the fourth step the eight conformations retained from step three were subjected to additional 500 iterations with DISMAN at level 46, whereby all dihedral angle constraints that did not correspond directly to a single, experimental spin-spin coupling constant were eliminated from the input. The resulting structures can thus be assessed against the directly measured NMR data. (The intermediary use of the supplementary dihedral angle constraints obtained from steps 1 and 2 is advantageous mainly because it tends to improve the convergence of the DISMAN calculations.) Overall this fourth step resulted only in small changes of the residual constraint violations and the molecular geometries relative to the results obtained in step 3.

In the final step the eight DISMAN solutions from step 4 were subjected to restrained energy minimi-

zation. The experimental restraints used correspond
to the input for step four (see above), except that the
distance constraints accounting for hydrogen bonds
and disulfide bridges were omitted, since these
bonds are allowed for by the energy force field. In
the program AMBER[30] the all-atom force field[31]
was modified by the following two additional terms:
Distance constraints from NOE measurements were
enforced by the potential:

$$A (d - u)^6, \text{ if } d > u \qquad (1)$$

where d is a proton-proton distance, u the upper
limit for this distance, and A a scaling factor such
that a violation $v = (d-u)$ of 0.2 Å corresponds to an
energy of kT/2 (see Fig. 2 of reference 32). Dihedral
angle constraints were enforced by the potential:

$$A [\sin (c\alpha + \alpha_0) + 1]^2,$$
$$\text{if } \alpha \text{ outside allowed range} \qquad (2)$$

where $\alpha$ is a dihedral angle, A a scaling factor which
assigns an energy of kT/2 to a value of $\alpha$ that is
outside of the allowed range by $v = 5°$, c converts the
periodicity of the sine function from $2\pi$ to the size of
the range of "forbidden" values of $\alpha$, and proper se-
lection of $\alpha_0$ ensures that the maximum value of the
potential is located at the center of the range of for-
bidden values of $\alpha$. [If $\alpha_u$ and $(\alpha_l - 2\pi)$ are the upper
and lower limits of the allowed range of the dihedral
angle $\alpha$, then $c = 2\pi/(\alpha_l - \alpha_u)$ and $\alpha_0 = -\pi/2 -
2\pi\alpha_u/(\alpha_l - \alpha_u)$.] A graphical illustration of this po-
tential is afforded by Figure 1. Overall, as is also
clearly visible from Figure 1, in Equations 1 and 2
large violations are strongly penalized, while viola-
tions smaller than v/2 have only negligibly small
effects.[32]

The AMBER minimizations were run on a CRAY
X-MP/28 until the RMSD change of the gradient
was smaller than 0.4 Å,[30] which required on the
average 653 iterations, or 71 seconds of CPU time.
In one DISMAN solution a large residual NOE-vio-
lation had to be relaxed interactively. Since this in-
volved only conformation changes of a single surface
side chain, it could readily be achieved with the mo-
lecular graphics program CONFOR.[33]

## RESULTS

The input for the distance geometry calculations*
was derived from the following experimental mea-
surements. A total of 263 distance constraints were
derived from the NOE data. Figure 2 shows the dis-
tribution of these constraints as a function of their
range on the level of the primary structure. Figure 3
shows the locations of all these NOE constraints in
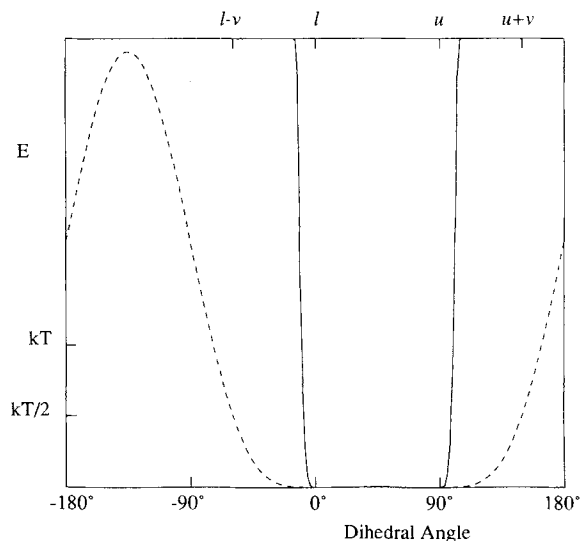one of the three-dimensional ATX Ia structures. In



Fig. 1. Potential representing the experimental dihedral angle
constraints in the modified AMBER force field (Eq. 2). l and u are
the lower and upper limits defining the allowed range for the tor-
sion angle. The two curves show potentials for different values of
v, where v is the violation of the allowed range of values for the
dihedral angle that corresponds to an energy of kT/2. The solid
line was calculated with $v = 5°$, i.e., with the value used for the
ATX Ia calculations. The broken line corresponds to $v = 60°$, and
it was included here to afford an overall view of the potential
function. The letters at the top identify the locations of the bounds
l and u for both potentials, and the dihedral angle violations (l − v)
and (u + v) corresponding to an energy of kT/2 in the dashed
curve.

addition to these distance constraints, 76 vicinal $^1$H-
$^1$H coupling constants (Table I) were obtained from
analysis of the cross peak fine structures in phase-
sensitive COSY, 2QF-COSY and 3QF-COSY spec-
tra.[4] Supplementary constraints were used to ac-
count for the hydrogen bonds indentified previously
in the regular secondary structures (Table II)[4] and
for the three disulfide bridges connecting the cystei-
nyl residues 4 and 43, 6 and 34, and 27 and 44.[4,10]

The type of results that were obtained from the
first step in the structural analysis of the experi-
mental data using the program HABAS[26] is illus-
trated in Figure 4. In this figure hatched bars indi-
cate allowed regions of $\phi$, $\psi$, and $\chi^1$ in selected
residues. Regions of the dihedral angles that are al-
lowed with respect to only one of the two possible
stereospecific assignments of the $\beta$-methylene pro-
tons are hatched either horizontally or vertically.
Cross-hatched areas indicate values accessible with
either of the two possible stereospecific assignments.
A stereospecific assignment by HABAS is achieved
if for any one of the three dihedral angles only hor-
izontal or only vertical hatching occurs. This is the
case for Cys 4 and Cys 6 in Figure 4. In all, the use
of HABAS resulted in eight stereospecific assign-
ments for $\beta$-methylene groups (Table III). Trp 31 is
worth noting since there are two well-separated re-
gions of $\chi^1$, each of which is allowed with one of the

---

*A detailed list of the experimental input data for the struc-
ture calculation will be deposited in the Brookhaven Protein
Data Bank, together with the atom coordinates.

**TABLE I. Scalar Coupling Constants $J_{HN\alpha}$ and $J_{\alpha\beta}$ Measured for ATX Ia**

| Residue | $J_{HN\alpha}$ | $J^*_{\alpha\beta}$ | $J^*_{\alpha\beta'}$ |
|---|---|---|---|
| | | Hz | |
| Cys 4 | 9.0 | 4.0 | 2.8 |
| Leu 5 | 8.5 | | |
| Cys 6 | 7.0 | 3.5 | 11.9 |
| Lys 7 | 5.7 | 6.0 | 10.0 |
| Ser 8 | 6.7 | 3.5 | 3.5 |
| Asp 9 | 7.2 | 3.5 | 11.4 |
| Asn 12 | 7.0 | | |
| Thr 13 | 6.5 | | |
| Arg 14 | 6.5 | 5.0 | 9.0 |
| Asn 16 | 7.5 | | |
| Ser 17 | 7.0 | | |
| Met 18 | 7.5 | 3.5 | 10.6 |
| Ser 19 | 10.0 | 3.5 | 3.5 |
| Thr 21 | 10.0 | 4.5 | |
| Ile 22 | 7.0 | 10.0 | |
| Trp 23 | 10.0 | 3.0 | 12.5 |
| Val 24 | 6.0 | | |
| Phe 25 | 8.5 | 3.5 | 12.0 |
| Cys 27 | 5.7 | 4.0 | 12.5 |
| Ser 29 | 5.5 | | |
| Trp 31 | 10.0 | 11.0 | 3.0 |
| Asn 32 | 9.2 | 3.5 | 12.0 |
| Asn 33 | 6.5 | 12.0 | 3.5 |
| Cys 34 | 10.0 | 3.5 | 3.5 |
| Glu 35 | 8.0 | 10.0 | 5.0 |
| Arg 37 | 7.7 | | |
| Ile 39 | 9.5 | 3.0 | |
| Ile 40 | 9.2 | 10.5 | |
| Tyr 42 | 8.0 | 3.0 | 11.0 |
| Cys 43 | 9.0 | 12.0 | 3.5 |
| Cys 44 | 10.2 | 12.0 | 5.0 |
| Lys 45 | 9.2 | 8.0 | 4.0 |

*Of the two β-methylene protons, β is observed at lower field than β'.

**TABLE II. Hydrogen Bonds That Were Identified in the Regular Secondary Structures of ATX Ia (Widmer et al., 1988[4]) and Included in the Input for the Distance Geometry Calculations**

| Donor | Acceptor | Occurrence* |
|---|---|---|
| Ile 22 HN | Ala 2 O' | 7 |
| Cys 4 HN | Gly 20 O' | 6 |
| Gly 20 HN | Cys 4 O' | 8 |
| Cys 6 HN | Ser 17 O' | 3 |
| Thr 21 HN | Cys 44 O' | 8 |
| Cys 44 HN | Thr 21 O' | 8 |
| Trp 23 HN | Tyr 42 O' | 7 |
| Tyr 42 HN | Trp 23 O' | 5 |
| Trp 31 HN | Pro 28 O' | 8 |
| Asn 32 HN | Lys 45 O' | 8 |
| Lys 45 HN | Asn 32 O' | 7 |
| Cys 34 HN | Cys 43 O' | 5 |
| Cys 43 HN | Cys 34 O' | 3 |

*This number indicates how many of the eight energy-refined DISMAN structures contained this hydrogen bond (see text for the search criteria used to identify hydrogen bonds.)

**TABLE III. Stereospecific Assignments for β-Methylene Groups in ATX Ia Obtained Prior to the DISMAN Calculations of the Three-Dimensional Structure***

| Residue | Method† | $\delta(H^{\beta 2})$ | $\delta(H^{\beta 3})$ |
|---|---|---|---|
| Cys 4 | HABAS | 3.16 | 3.03 |
| Cys 6 | HABAS | 2.51 | 3.37 |
| Lys 7 | HABAS | 1.91 | 2.36 |
| Asp 9 | HABAS | 3.05 | 2.97 |
| Arg 14 | HABAS | 1.93 | 1.80 |
| Trp 23 | Statistics | 2.71 | 3.30 |
| Phe 25 | Statistics | 2.98 | 3.50 |
| Cys 27 | HABAS | 2.64 | 2.53 |
| Trp 31 | Statistics | 3.10 | 2.76 |
| Asn 32 | Statistics | 2.75 | 2.68 |
| Cys 43 | HABAS | 2.68 | 2.99 |
| Lys 45 | HABAS | 1.97 | 2.03 |

*The total number of β-methylene groups in ATX Ia is 27.
†HABAS indicates stereospecific assignments obtained by applying the program HABAS (Güntert et al., 1989[26]), which uses only intraresidual and sequential NMR constraints; Statistics indicates stereospecific assignments based on the analysis of 500 DISMAN calculations up to level 5, which uses intraresidual, sequential, and medium-range NMR constraints.

would be obtained. In contrast, Cys 34 is a case with little hope of obtaining such assignments, since the regions that are allowed for the two stereospecific assignments are overlapped. For all residues, irrespective of whether stereospecific assignments could be obtained and including those with a single β-proton, HABAS provided dihedral angle constraints as a first interpretation of the local experimental constraints.

The analysis of the results of 500 DISMAN calculations pursued to level 5, i.e., using all intraresidual, sequential, and medium-range constraints, resulted for a number of residues in very narrow confinements of the dihedral angles. As an example, Figure 5 shows the distribution of values for $\chi^1$ and $\chi^2$ of Trp 31 among 396 locally converged conformers. From such data one can again define dihedral angle constraints that are based on a statistically significant number of searches in conformation space. Furthermore, Figure 5 shows that $\chi^1$ of Trp 31 adopted only values around $-60°$, which corresponds to the allowed range of $\chi^1$ for one of the two stereospecific assignments, while the other one would require $\chi^1$-values near 180° (Fig. 4). As a result βCH$_2$ of Trp 31 could be stereospecifically assigned (Table III). Figure 6 displays the fragment 27–31 in the energy-refined DISMAN structure 1, and all the distance constraints within it. It is readily apparent that only a limited range of conformation space is accessible for the side chain of Trp 31. In all, stereospecific assignments for four additional β-methylene groups were thus obtained (Table III). The total of 12 stereospecific assignments obtained in the first two steps of the analysis corresponds to 45% of all β-methylene groups in ATX Ia.

two possible assignments. Should additional, longer-range constraints discriminate against one of these regions, stereospecific assignments for this residue
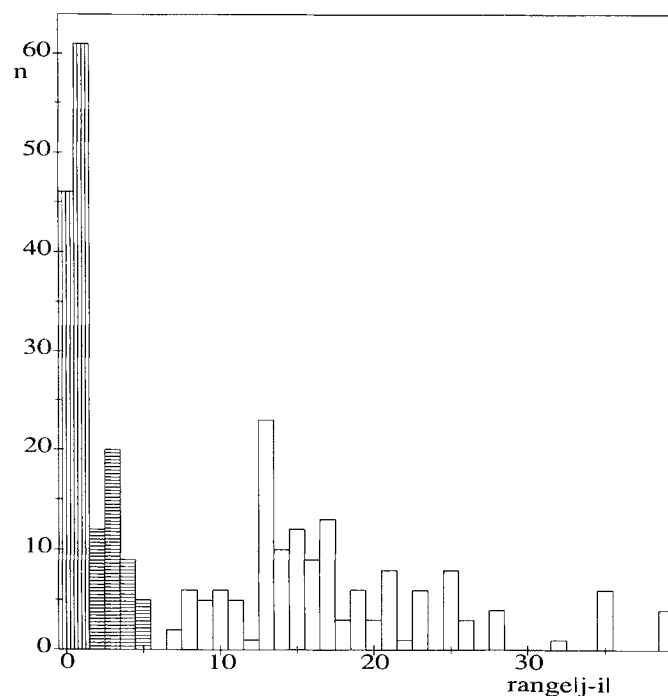
Fig. 2. Distribution of the number of NOE distance constraints versus their range along the amino acid sequence. $i$ and $j$ are the sequence positions of the two interacting residues. The vertically hatched bars represent the intraresidual and sequential NOE's; the horizontally hatched and open bars, respectively, indicate medium- and long-range NOE's.[27]
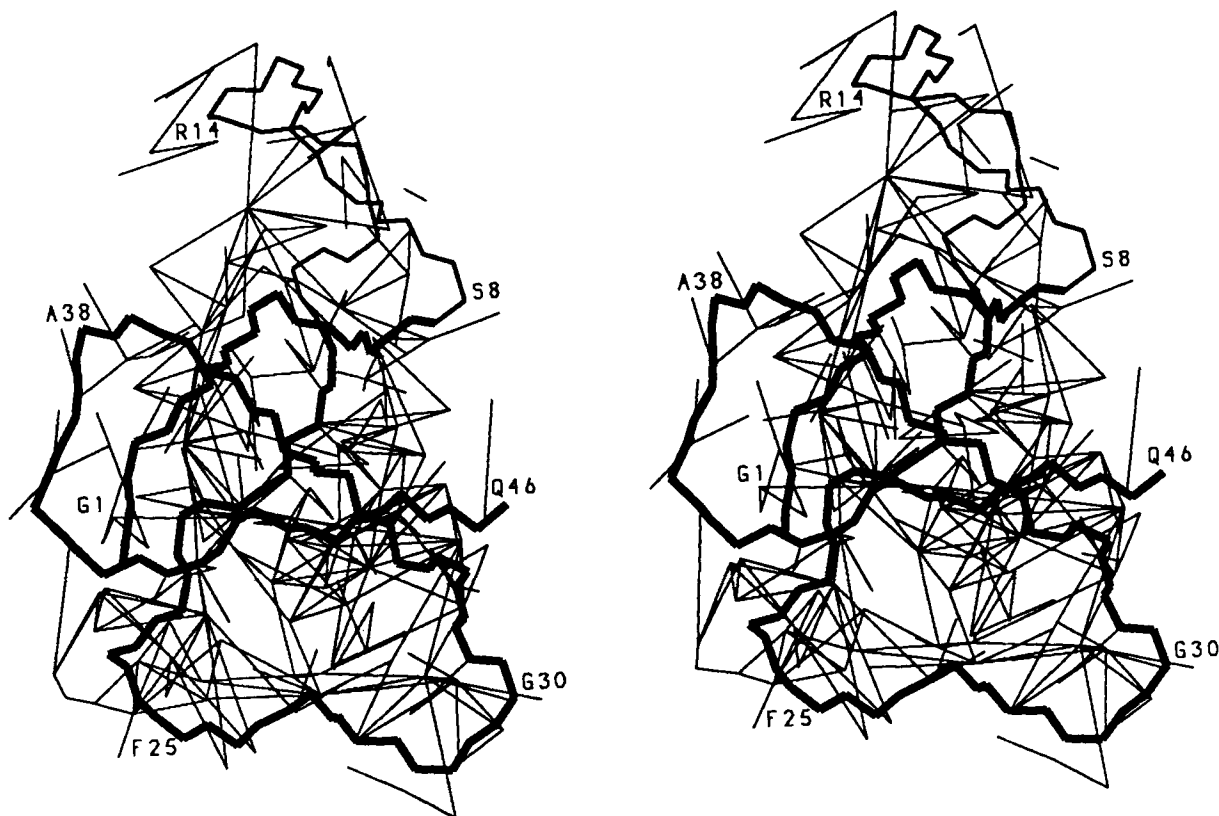


Fig. 3. Pictorial presentation of the NOE distance constraints used for the structure calculation. A heavy line traces the backbone of the energy-refined DISMAN structure 1, where the disordered loop of residues 8–18 is shown with a somewhat lighter line. Thin lines connect hydrogen atom and pseudoatom positions between which a NOE was observed, including those in the side chains. The low density of NOE's in the upper part of this projection correlates with the apparent structural disorder for residues 8–18 in the structures calculated from the NMR data. In this stereo view the locations of selected amino acid residues have been identified by the one-letter code and the sequence position.

### TABLE IV. Residual Constraint Violations and Conformational Energies of the Eight DISMAN Structures of ATX Ia Before and After Energy Refinement

| Structure* | Residual constraint violations† | | | | Energy (kcal/mol) |
|---|---|---|---|---|---|
| | $d^{\ddagger}_{max}$ >0.2 Å | $d^{\ddagger}_{min}$ >0.2 Å | dih.angle >5.0° | vdW >0.2 Å | |
| D1 | 2 (0.25) | 0 (0.16) | 0 (2.1) | 0 (0.19) | −16 |
| D2 | 7 (0.57) | 2 (0.56) | 1 (6.8) | 3 (0.36) | 183 |
| D3 | 13 (0.50) | 2 (0.41 | 1 (6.5) | 2 (0.33) | 286 |
| D4 | 6 (0.49) | 4 (0.39) | 2 (6.9) | 4 (0.32) | 143 |
| D5 | 5 (0.39) | 1 (0.23) | 1 (6.0) | 1 (0.35) | 138 |
| D6 | 10 (0.57) | 2 (0.30) | 2 (10.0) | 4 (0.30) | 304 |
| D7 | 7 (0.30) | 1 (0.34) | 0 (2.8) | 1 (0.21) | 115 |
| D8 | 2 (0.24) | 3 (0.41) | 0 (2.4) | 0 (0.12) | 147 |
| $\bar{D}$ | 6.5 (0.41) | 1.9 (0.35) | 0.9 (5.4) | 1.9 (0.27) | 163 |
| A1 | 0 (0.19) | 0 (0.12) | 2 (5.9) | 0 (0.14) | −543 |
| A2 | 2 (0.21) | 0 (0.16) | 2 (5.9) | 0 (0.18) | −444 |
| A3 | 6 (0.23) | 0 (0.15) | 1 (5.0) | 0 (0.13) | −459 |
| A4 (mod.) | 1 (0.20) | 0 (0.06) | 3 (5.6) | 0 (0.18) | −484 |
| A5 | 3 (0.21) | 0 (0.06) | 3 (5.6) | 0 (0.08) | −437 |
| A6 | 2 (0.21) | 0 (0.06) | 2 (6.9) | 0 (0.13) | −444 |
| A7 | 5 (0.21) | 0 (0.07) | 1 (5.7) | 0 (0.09) | −518 |
| A8 | 1 (0.20) | 0 (0.09) | 4 (6.1) | 1 (0.26) | −473 |
| $\bar{A}$ | 2.5 (0.21) | 0 (0.10) | 2.3 (5.8) | 0.1 (0.15) | −475 |

*$D_i$ and $A_i$ indicate, respectively, individual ones of the eight DISMAN structures before and after energy refinement with the program AMBER. $\bar{D}$ and $\bar{A}$ are the averages of the numbers for the structures $D_i$ and $A_i$, respectively. mod. indicates that a special procedure was used in the refinement of structure 4 (see text).

†$d_{max}$ are upper distance limits obtained from NOE's and used to define hydrogen bonds and disulfide bonds. $d_{min}$ are lower distance limits used to define hydrogen bonds and disulfide bonds. dih.angle are constraints on the dihedral angles $\phi$, $\psi$, and $\chi^1$ obtained from combined analysis of intraresidual and sequential NOE constraints and experimental values of $^3J_{HN\alpha}$ and $^3J_{\alpha\beta}$ with the program HABAS. vdW are van der Waals contacts evaluated using the atomic radii defined in the DISMAN program. The numbers in parentheses indicate the largest individual violations.

‡The constraints $d_{min}$ and $d_{max}$ that define hydrogen bonds and disulfide bonds were explicitly included only during the DISMAN calculations.

In steps 3 and 4 we used the program DISMAN[28] to compute the complete three-dimensional structure, as described in the Computational Procedures section. Eight of the initially started 100 runs were completed and converged to conformers with only small residual violations of the experimental NMR constraints (Table IV). The conformational energy of these eight species was, however, rather high, since interactions such as electrostatic attraction or repulsion are not considered by DISMAN. Therefore restrained energy refinement with a modified version of AMBER[30] was added as a last step of the structure determination. Table IV shows that besides a net improvement in energy, the residual violations of the experimental constraints could be kept at the same value or were even decreased.

When we tried to superimpose the eight energy-refined DISMAN structures for minimal RMSD, it was readily apparent that different regions of the polypeptide chain are defined with different precision (Fig. 7). The polypeptide backbone of residues 1–7 and 19–46 is well defined, with an average RMSD value of 1.4 Å between all structure pairs (Table V), while the loop including the residues 8–18 spans a significantly wider conformational space. A schematic drawing of ATX Ia is shown in Figure

### TABLE V. Average of the Minimal Pairwise RMSD's Among the Eight DISMAN Solutions for ATX Ia After Energy Minimization With the Program AMBER

| Atoms used to calculate RMSD | $\overline{RMSD}$ |
|---|---|
| Backbone of residues 1–7, 19–46* | 1.4 ± 0.3 |
| Same plus interior sidechains† | 1.5 ± 0.3 |
| Complete backbone 1–46* | 2.7 ± 0.9 |
| All heavy atoms of residues 1–46 | 3.6 ± 0.8 |

*Backbone atoms are N, $C^{\alpha}$, C', and O'.
†Interior side chains in the polypeptide segments 1–7 and 19–46 are 3–6, 19–23, 26–28, 31, 34, 36, 39, 41, 43–45. The selection criterium used was that on the average in the eight structures, less than 30% of the residue surface is exposed to the solvent.

8, which displays the β-sheet, the disulfide bridges and the flexible loop. The polypeptide chain arrangement forms a highly twisted, right-handed β-sheet. This antiparallel sheet consists of four strands including the residues 2–7, 19–24, 31–34, and 41–46, which are connected by the poorly determined loop 8–18 and the well-defined loops 25–30 and 35–40. Figure 9 affords an impression of the extent to which the local structure including the amino acid side chains is uniquely and precisely de-
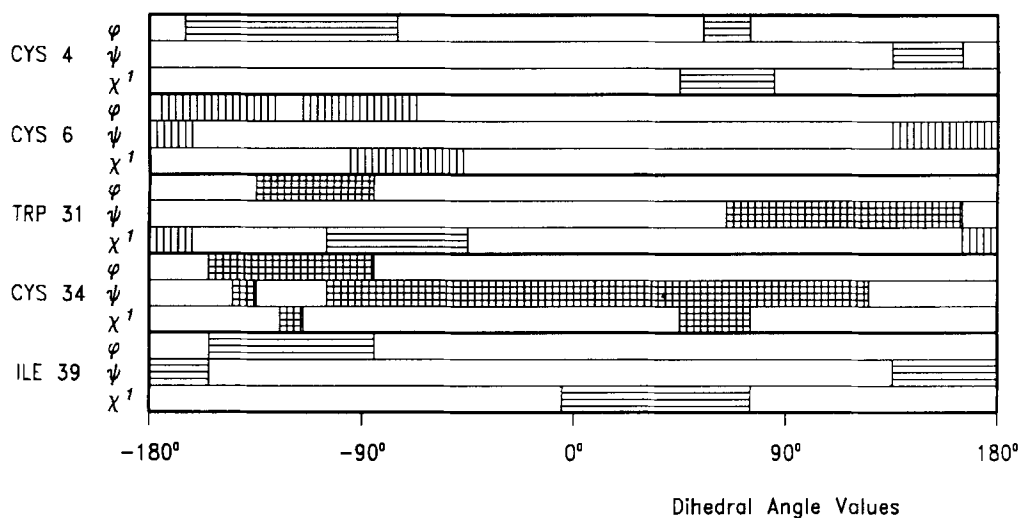
Fig. 4. Some examples of results obtained with the program HABAS.[26] For each of the dihedral angles $\phi$, $\psi$, and $\chi^1$ the ranges that are allowed relative to the experimental spin-spin coupling constants and the intraresidual and sequential NOE's are given by hatched bars. Horizontal hatching corresponds to one of the two stereospecific assignments and vertical hatching to the other one. Double hatched bars indicate angle values accessible for both possible stereospecific assignments. For Ile 39, HABAS was used only to determine the allowed ranges for the dihedral angles.
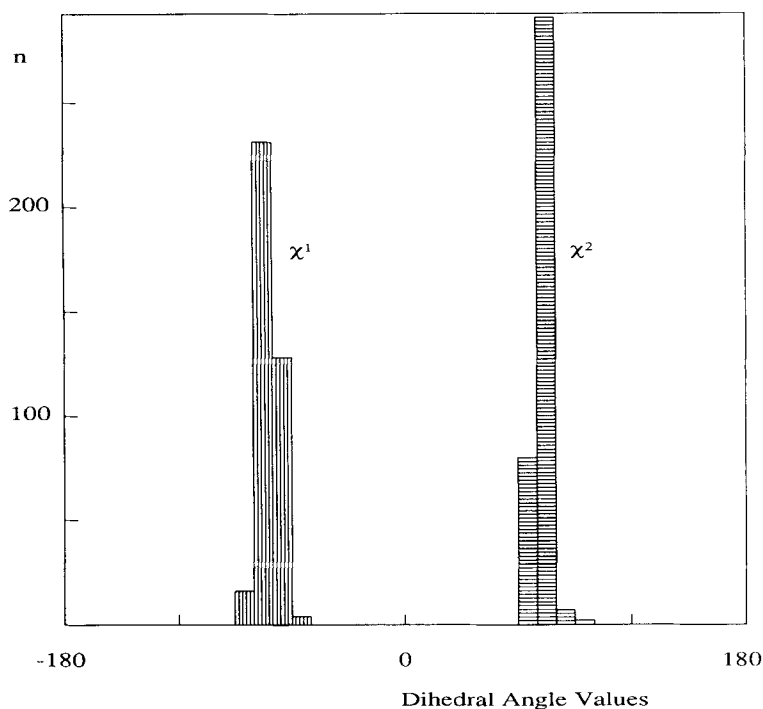


Fig. 5. Distribution of the values found for the dihedral angles $\chi^1$ (vertical hatching) and $\chi^2$ (horizontal hatching) of Trp 31 in the 396 structures obtained in step two of the structure determination (see text) which converged locally for residues 30–32. These 396 structures thus show no significant residual violations of any short-range or medium-range distance constraints or steric constraints involving residues 30–32, and similarly, except for very small violations, all dihedral angle constraints in this fragment are satisfied.
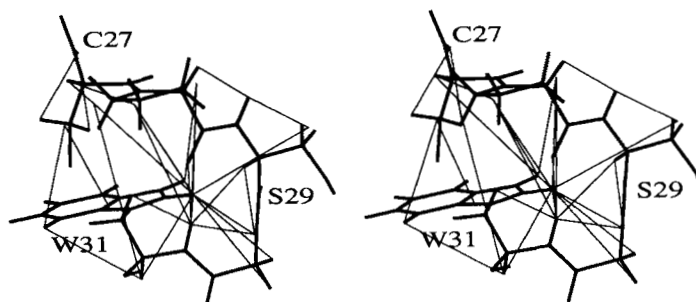
Fig. 6. Stereo view of the conformation of the residues 27–31 in the energy refined DISMAN structure 1 (heavy lines) with all NOE distance constraints that were observed within this fragment (thin lines).
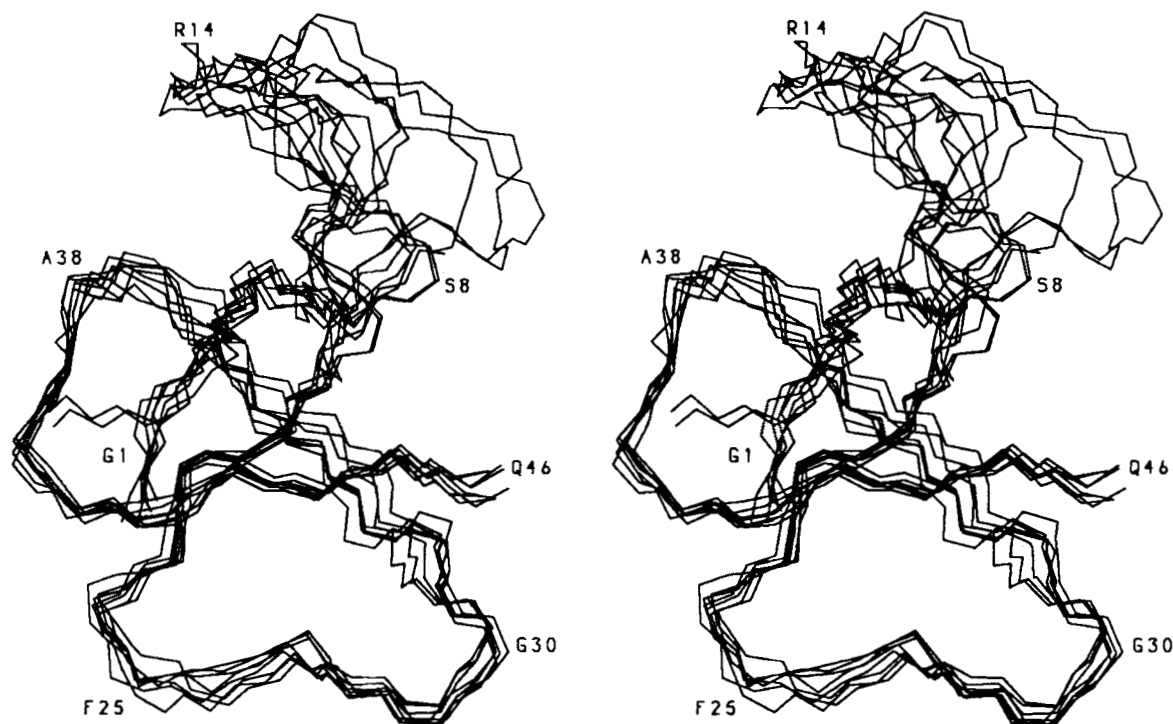


Fig. 7. Superposition of the polypeptide backbone in the eight energy-refined DISMAN structures of ATX Ia. The structures were superimposed for pairwise minimal RMSD with structure 1, where the backbone atoms N, C$^\alpha$, and C' of residues 1–7 and 19–46 were used for the calculation of the RMSD. In this stereo presentation the flexible loop consisting of residues 8–18 is at the top of the structure, and the same residues are identified as in Figure 3.

fined. Each of the four polypeptide segments shown contains one of the β-strands. Many side chains are well defined, including the bulky aromatic residues Trp 23 and Trp 31. For other side chains, such as Phe 25 or Tyr 42, which are located near the protein surface, it is readily apparent that no unique spatial orientation was defined by the NMR data.

## DISCUSSION

In the present investigation of the neurotoxin ATX Ia, several novel procedures have been applied for the first time in a determination of the three-dimensional structure of a protein. The initial two steps of the structure calculations using the program HABAS and DISMAN sampling up to level 5 are devised so as to ensure that all conformations consistent with the experimental short-range and medium-range constraints will be found. For the intraresidual and sequential constraints this was achieved with the program HABAS by a grid search, and for the medium-range constraints by extensive DISMAN sampling of approximately 100–500 structures, depending on the residue considered. These procedures allow a thorough check of the internal consistency of the ensemble of all experimental and steric constraints. For example, in the case of ATX
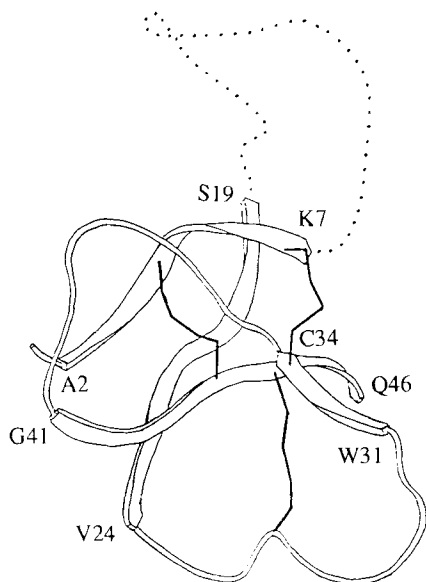
Fig. 8. Schematic drawing of the solution structure of ATX Ia in the same orientation of the molecule as in Figure 7, indicating the location of the four β-strands, the flexible loop (dotted), and the three disulfide bridges (heavy lines). For each β-strand the first and the last residue are identified by the one-letter symbol and the sequence position.

Ia we removed all intraresidual constraints $d_{\alpha\beta}$ (i,i) from the input list because they were often incompatible with the other data, presumably because zero-quantum contributions to these cross-peaks may have falsified the NOE intensity assessment of the $d_{\alpha\beta}$ cross-peaks.[27] These complete searches of the conformation space can further yield stereospecific assignments of β-methylene groups, and they provide good starting structures for the continued structure calculations. Although these starting structures are biased toward locally correct conformations, which may improve the convergence of subsequent DISMAN calculations, they do not discriminate between different groups of structures that may be obtained as the final result of the calculations.

For the final step of restrained energy refinement, the energy force field AMBER[31] has been supplemented with additional potentials for the experimental constraints, i.e., for upper distance limits and bounds on the allowed dihedral angle ranges (Eqs. 1, 2; Fig. 1). The results in Table IV show that besides the minimization of the conformational energy, a significant reduction of the residual violations of NOE distance bounds was achieved. This reduction of the residual distance violations with respect to the DISMAN solutions is to a large part also a consequence of working in the Euclidian space of atomic coordinates during the AMBER energy minimization, as compared to the computations in dihedral angle space in the DISMAN program, as this

increases the number of degrees of freedom. In contrast to the distance constraints, the extent of the residual violations of the dihedral angle constraints was nearly unchanged. This is not surprising if one considers that most of these violations were already smaller than v = 5° (Table IV), which corresponds to an energy of kT/2 (Eq. 2). In the energy-refined structures the average deviation of the bond lengths from the ideal values is 0.007 Å, with maximal deviations ranging from 0.02 to 0.03 Å in the individual eight structures. For the bond angles the average deviations is 1.6°, with maxima ranging from 5.2° to 11.7° in the eight structures. These deviations are of the same magnitude as the differences between the ideal covalent geometries defined by different, commonly used force fields.[32] The ω dihedral angles about the peptide bonds were kept rigid at 180° during the DISMAN calculations. The energy-refined structures show an average deviation of the ω angles of 5°, with maximal deviations between 12° and 19° for the eight structures. This seems acceptable, in particular when compared with experimentally observed deviations in peptide and protein crystal structures. For example, in the high resolution crystal structure of the dipeptide α-L-Glu-L-Asp an ω angle of 161.3° was explained by hydrogen bonding between the protonated Glu side chain and the C-terminal carboxyl group mediated by a water molecule.[34]

A remarkable feature of the solution conformation of ATX Ia represented by the group of eight DISMAN structures is the poorly defined loop which connects the first and the second β-strand. To locate this disordered loop precisely in the sequence, local RMSD values[35] were calculated for all pentapeptide segments in the protein and plotted as a function of the sequence (Fig. 10). The loop was then defined so as to include all residues with local RMSD values in excess of 1.0 Å, i.e., residues 8–18. This location of the disordered loop is also supported by the quantitative comparisons of the eight conformers in Table V. The average of the RMSD values for the backbone atoms of residues 1–7 and 19–46 is 1.4 Å. Nearly the same precision is obtained if one includes 20 "interior" side chains selected on the basis that less than 30% of their surface is exposed to the solvent. Figure 11 presents an illustration of the compact packing in the core of the protein consisting of the polypeptide backbone segments 1–7 and 19–46, and these interior side chains. If the flexible loop is also considered, the backbone comparison has a significantly higher RMSD value of 2.7 Å, and for all heavy atoms a value of 3.6 Å is obtained.

Figure 12 provides further insights into the architecture of the ATX Ia molecule. A core of disulphide bridges (Fig. 12A, heavy lines) is surrounded on one side by hydrophobic residues (medium lines), and on the other side by hydrophilic residues (thin lines). Figure 12B shows the location of intramolecular hy-
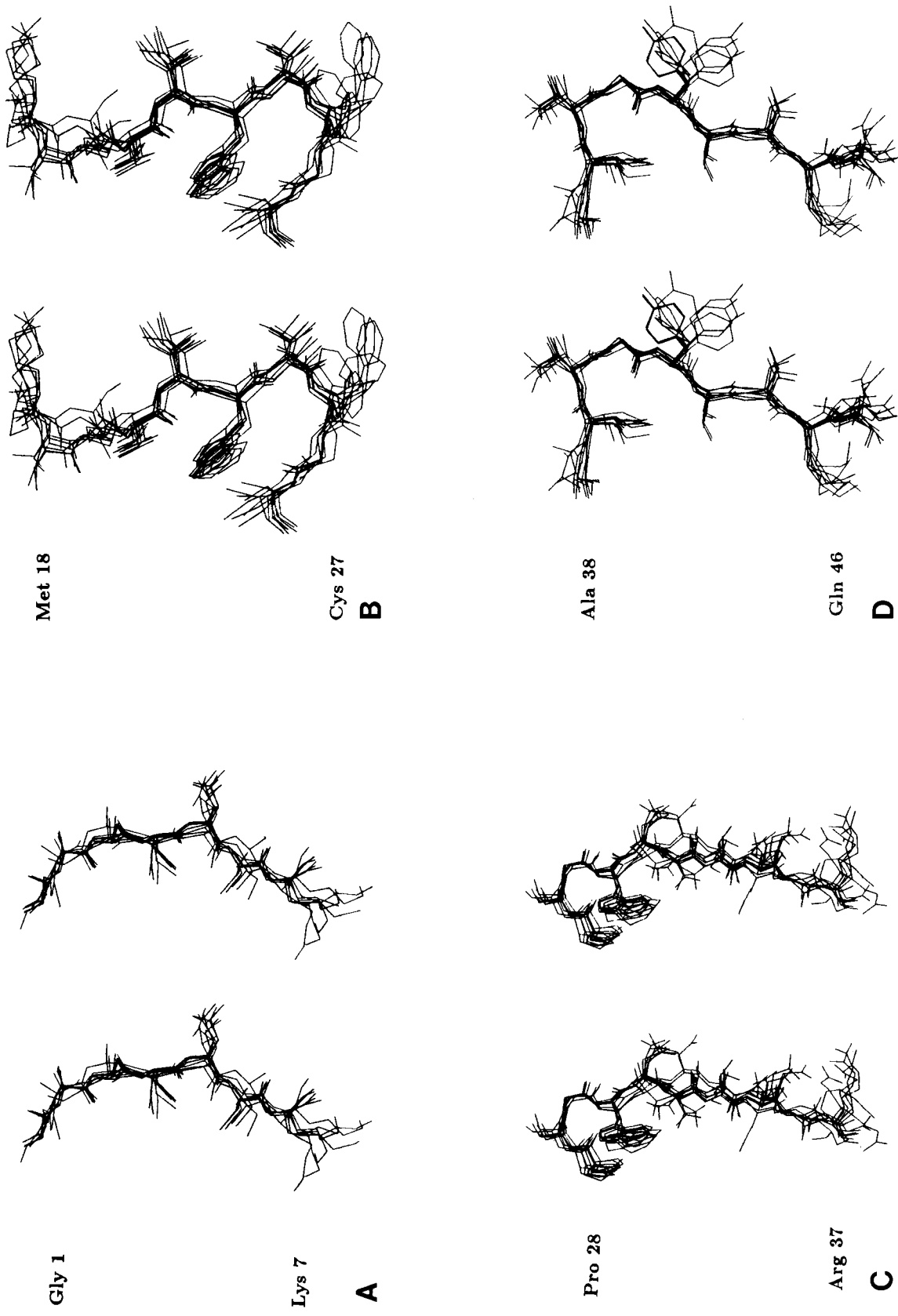
Gly 1

Lys 7

**A**

Met 18

Cys 27

**B**

Pro 28

Arg 37

**C**

Ala 38

Gln 46

**D**

Fig. 9. Stereo views of the eight energy-refined DISMAN structures of ATX la as local superpositions for minimum pairwise RMSD relative to structure 1 calculated for the backbone atoms N, C$^\alpha$, and C' of the fragments 1–7 (**A**), 18–27 (**B**), 28–37 (**C**), and 38–46 (**D**).
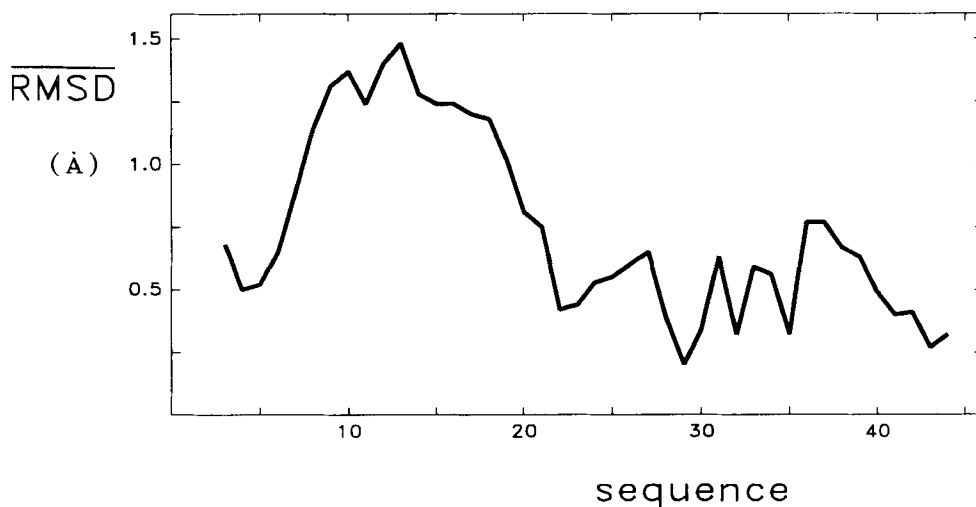
Fig. 10. Differences in local conformation among the eight energy-refined DISMAN structures of ATX Ia. For all corresponding pentapeptide fragments in these structures the minimal pair-wise RMSD's were calculated for the N, $C^{\alpha}$, and C' atoms. The average of these RMSD's was then plotted at the position of the central residue of each pentapeptide.
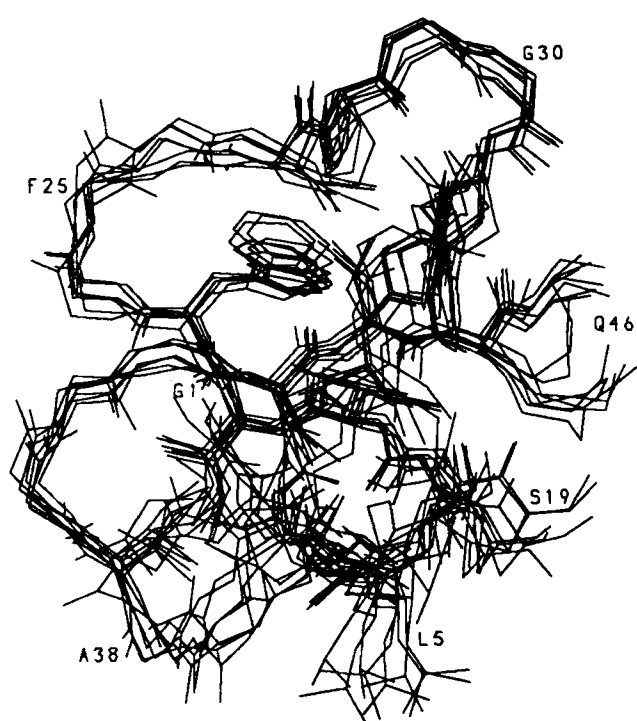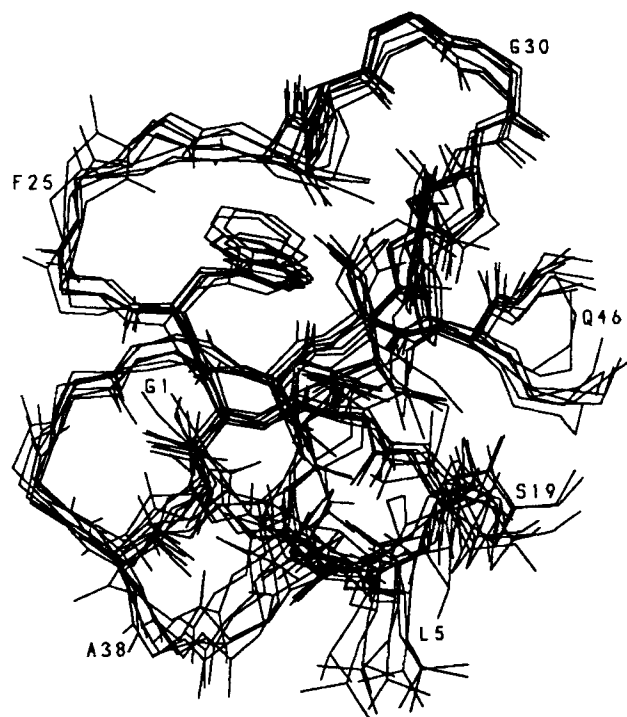


Fig. 11. Stereo view of the eight energy-refined DISMAN structures of ATX Ia shown in Figure 7. The figure shows the polypeptide backbone of the residues 1-7 and 19-46 as well as the side chain heavy atoms of all interior residues in these two segments (see footnote to Table V for the selection of the interior residues). In this orientation of the molecule the flexible loop 8-18 would be on the lower right side.

drogen bonds (solid heavy lines) and electrostatic interactions (broken heavy lines), which were identified with the following selection criteria: A hydrogen bond was accepted as such if in more than four of the eight energy-refined DISMAN structures the distance from the donor hydrogen to the acceptor atom was smaller than 2.4 Å, and the angle between the covalent bond linking the hydrogen to the donor group and a line connecting the donor and acceptor groups was smaller than 35°. Electrostatic interac-
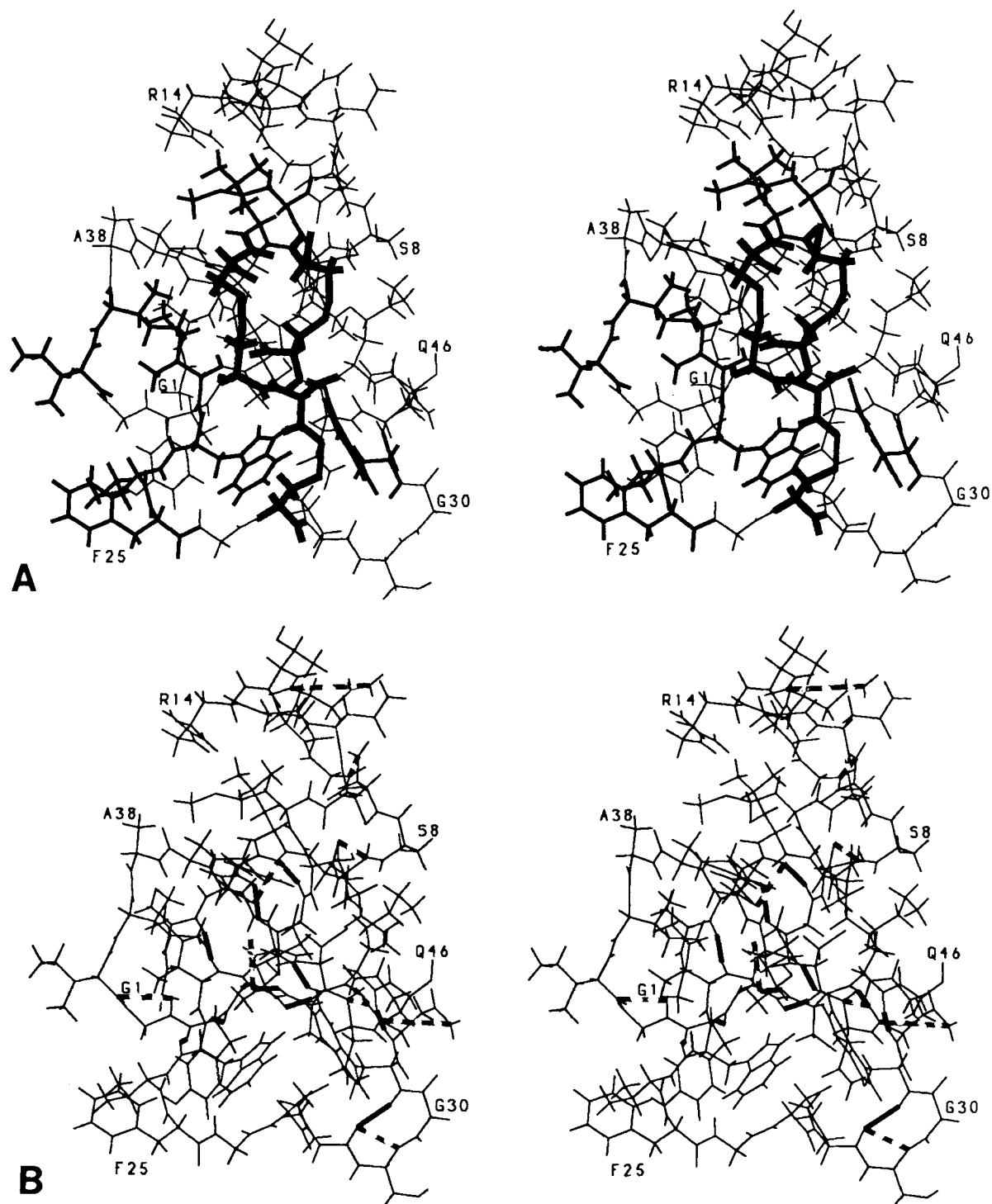
Fig. 12. Pictorial presentation of the distribution of hydropho-
bic residues, hydrogen bonds and charged groups in ATX Ia in a
stereo view of the energy-refined DISMAN structure 1. The same
residues are identified as in Figure 3. **A:** Cysteinyl residues are
drawn with heavy lines; the hydrophobic residues Ile, Leu, Met,
Phe, Trp, and Val are shown with medium lines; and all other
residues with thin lines. **B:** Hydrogen bonds are displayed with
solid heavy lines; strongly attractive electrostatic interactions with
broken heavy lines. These bonds are shown if they occur in at
least four of the eight energy-refined DISMAN structures (see text
for the criteria used to identify these interactions in the individual
structures).

tions were accepted if their attractive force according to the AMBER force field[31] exceeded 10 kcal/mol in more than four of the structures. All but two of the 13 hydrogen bonds that were identified previously[4] in the direct secondary structure determination from NMR data (Table II) satisfied these criteria, and no additional hydrogen bonds were unambiguously identified by these criteria (see below). Table II shows that the hydrogen bonds involve predominantly backbone atoms of residues with hydrophobic side chains. Four of the nine electrostatic interactions shown in Figure 12B are between hydrophilic residues and cysteines, and another four are between different hydrophilic residues. The two previously identified hydrogen bonds[4] that are now questionable in view of the complete structure determination, are those from Cys 6 to Ser 17, and from Cys 43 to Cys 34. They are located at the very end of the β-sheets (Fig. 8), so that it is not really surprising that they are less well defined than the more interior hydrogen bonds.

Besides the uncertainty in the identification of the hydrogen bond of Ser 17 O' with Cys 6 NH, there is additional evidence for local conformational polymorphism near the transition from the well-structured protein core to the disordered loop 8–18. This includes that the outstanding low field chemical shift of 10.11 ppm for the amide proton of Ser 19[4] is indicative of hydrogen bonding,[36] although this residue is not involved in the regular hydrogen bonding network of the β-sheet, and the proton exchanges rapidly with the solvent.[4] The amide proton resonance of Ser 19 is also significantly broadened, which would be compatible with exchange between two or several conformational states. Using the aforementioned criteria, we identified a hydrogen bond between Ser 17 O' and Ser 19 NH in four of the eight energy-refined ATX Ia structures, showing that the interactions of Ser 17 O' with the amide protons of either Cys 6 or Ser 19 are about equally probable (see Table II). (In the previous direct secondary structure identification in ATX Ia these apparent nonregular features of the β-sheet were interpreted as indicating the presence of a β-bulge[4].)

As mentionned in the Introduction, the solution conformations of several sea anemone neurotoxins that are homologous to ATX Ia are currently under investigation. However, as only preliminary, incomplete descriptions of other three-dimensional structures have as yet been presented, only a preliminary comparison with ATX Ia is possible. The backbone folds of anthopleurin-A from *Anthopleura xanthogrammica*[9] and RpII from *Radianthus paumontensis*[37] are very similar to ATX Ia (Figs. 7, 8). Furthermore, a detailed view of the interior side chains of Thr 21, Trp 23 and Trp 33 (the latter corresponds to Trp 31 in ATX Ia) given by Torda et al.[9] for anthopleurin-A concides well with the ATX Ia structure, where the conformation of Trp 23 and especially of Thr 21 is quite precisely defined (Fig. 9B). In view of the fact aht all these homologous toxins appear to have closely similar three-dimensional structures, it is interesting to note that the residues which are strictly conserved among 10 known variants[7] include not only seven locations in the well structured protein core, i.e., the six cysteines and Trp 31 (in the numeration of ATX Ia), but also Gly 11, Pro 12, and Arg 14 in the disordered loop. This might be taken as an indication of a special functional role of the flexible loop for the biological activity of these neurotoxins, for example, in the recognition of and/or binding to the receptor.[7]

A more complete comparison is warranted between ATX Ia and the antihypertensive and antiviral polypeptide BDS-I,[11,12] since complete structure determinations are available for both proteins. The 30% sequence homology between ATX Ia and BDS-I is reflected in some similarities of the global architectures. The relative spatial arrangements of the three disulfide bridges and of three strands of the β-sheet is closely similar in the two proteins. In contrast, the amino terminal β-strand in ATX Ia is missing in BDS-I, and the twist of the β-sheet is significantly more pronounced in ATX Ia than in BDS-I. A common detail of the two structures are the side chain interactions between Trp 23, Pro 28, and Trp 31 in ATX Ia, and the corresponding residues Trp 16, Pro 23, and Tyr 28 in BDS-I. Significant differences are seen in the length and the conformation of the loops which connect the β-strands. The flexible loop between the first two β-strands of ATX Ia is substituted in BDS-I by a peptide segment that is about 7 residues shorter and forms a well defined, miniature antiparallel β-sheet and a type II turn. The loop between the second and third β-strands in BDS-I contains the 14 residues 17–30, whereas the corresponding loop in ATX Ia contains only the 6 residues 25–30. In ATX Ia the loop leading to the C-terminal β-strand consists of the 6 residues 35–40, whereas the corresponding loop in BDS-I is very tight due to a cis-peptide bond at Pro 36. Finally, while the fourth β-strand in ATX Ia extends to the end of the polypeptide chain, the three C-terminal residues of BDS-I form another turn. Overall, in spite of some readily apparent common traits in the molecular architectures of ATX Ia and BDS-I, there are pronounced, extensive structural differences that may in the future be more directly related with the different physiological functions of the two proteins.

## ACKNOWLEDGMENTS

# REFERENCES

1. Beress, L. Sea anemone toxins; a minireview. In: "Chemistry of Peptides and Proteins," Vol. 1. Voelter, W., Wünsch, E., Ovchinnikov, J., Ivanov, V. (eds.). Berlin: Walter de Gruyter & Co., 1982:121–126.

2. Wunderer, G. "Biologisch Aktive Polypeptide aus der Seeanemone *Anemonia sulcata*. Neurotoxine und Breitspezifische Proteinase-Inhibitoren: Isolierungen, Charakterisierungen, Sequenzen." Dissertation, Technische Universität München, 1975.

3. Gooley, P.R., Norton, R.S. Specific assignment of resonances in the $^1$H-NMR spectrum of the polypeptide toxin I from *Anemonia sulcata*. Biopolymers 25:489–506, 1986.

4. Widmer, H., Wagner, G., Schweitz, H., Lazdunski, M., Wüthrich, K. The secondary structure of the toxin ATX Ia from *Anemonia sulcata* in aqueous solution determined on the basis of complete sequence-specific $^1$H-NMR assignments. Eur. J. Biochem. 171:177–192, 1988.

5. Gooley, P.R., Norton, R.S. Specific assignment of resonances in the $^1$H nuclear magnetic resonance spectrum of the polypeptide cardiac stimulant *anthopleurin-A*. Eur. J. Biochem. 153:529–539, 1985.

6. Wemmer, D.E., Kumar, N.V., Metrione, R.M., Lazdunski, M., Drobny, G., Kallenbach, N.R. NMR analysis and sequence of toxin II from the sea anemone *Radianthus paumotensis*. Biochemistry 25:6842–6849, 1986.

7. Pease, J.H.B., Kumar, N.V., Schweitz, H., Kallenbach, N.R., Wemmer, D.E. NMR studies of toxin III from the sea anemone *Radianthus paumotensis* and comparison of its secondary structure with related toxins. Biochemistry 28:2199–2204, 1989.

8. Fogh, R.H., Mabbutt, B.C., Kem, W.R., Norton, R.S. Sequence-specific $^1$H NMR assignments and secondary structure in the sea anemone polypeptide *Stichodactyla helianthus* neurotoxin I. Biochemistry 28:1826–1834, 1989.

9. Torda, A.E., Mabbutt, B.C., van Gunsteren W.F., Norton, R.S. Backbone folding of the polypeptide cardiac stimulant *anthopleurin-A* determined by nuclear magnetic resonance, distance geometry and molecular dynamics. FEBS Lett. 239:266–270, 198.

10. Wunderer, G. Die Disulfidbrücken von Toxin II aus *Anemonia sulcata*. Hoppe Seylers Z. Physiol. Chem. 359: 1193–1201, 1978.

11. Driscoll, P.C., Clore, G.M., Beress, L., Gronenborn, A.M. A proton nuclear magnetic resonance study of the antihypertensive and antiviral protein BDS-I from the sea anemone *Anemonia sulcata*: Sequential and stereospecific resonance assignment and secondary structure. Biochemistry 28:2178–2187, 1989.

12. Driscoll, P.C., Gronenborn, A.M., Beress, L., Clore, G.M. Determination of the three-dimensional solution structure of the antihypertensive and antiviral protein BDS-I from the sea anemone Anemonia sulcata: A study using nuclear magnetic resonance and hybrid distance geometry-dynamical simulated annealing. Biochemistry 28:2188–2189, 1989.

13. Wunderer, G., Eulitz, M. Amino-acid sequence of toxin I from *Anemonia sulcata*. Eur. J. Biochem. 89:11–17, 1978.

14. Braun, W. Distance geometry and related methods for protein structure determination from NMR data. Q. Rev. Biophys. 19:115–157, 1987.

15. Schweitz, H., Vincent, J.-P., Barhanin, J., Frelin, Ch., Linden, G., Hugues, M., Lazdunski, M. Purification and pharmacological properties of eight sea anemone toxins from *Anemonia sulcata, Anthopleura xanthogrammica, Stoichactis giganteus,* and *Actinodendron plumosum*. Biochemistry 20:5245–5252, 1981.

16. Anil-Kumar, Ernst, R.R., Wüthrich, K. A two-dimensional nuclear overhauser enhancement (2D NOE) experiment for the elucidation of complete proton-proton cross-relax-

17. Bothner-By, A.A., Stephens, R.L., Lee, J., Warren, C.D., Jeanloz, R.W. Structure determination of a tetrasaccharide: Transient nuclear Overhauser effects in the rotating frame. J. Am. Chem. Soc. 106:811–813, 1984.

18. Bax, A., Sklenar, V., Summers, M.F. Direct identification of relayed nuclear overhauser effects. J. Magn. Reson. 70: 327–331, 1986.

19. Kessler, H., Griesinger, C., Kerssebaum, R., Wagner, K., Ernst, R.R. Separation of gross-relaxation and J cross-peaks in 2D rotating-frame NMR spectroscopy. J. Am. Chem. Soc. 109:607–609, 1987.

20. Marion, D., Wüthrich, K. Application of phase sensitive two-dimensional correlated spectroscopy (COSY) for measurements of $^1$H-$^1$H spin-spin coupling constants in proteins. Biochem. Biophys. Res. Commun. 113:967–974, 1983.

21. DeMarco, A., Wüthrich, K. Digital filtering with a sinusoidal window function: An alternative technique for resolution enhancement in FT NMR. J. Magn. Reson. 24:201–204, 1976.

22. Otting, G., Widmer, H., Wagner, G., Wüthrich, K. Origin of $t_1$ and $t_2$ ridges in 2D NMR spectra and procedures for suppression. J. Magn. Reson. 66:187–193, 1986.

23. Billeter, M., Braun, W., Wüthrich, K. Sequential resonance assignments in protein $^1$H nuclear magnetic resonance spectra. Computation of sterically allowed proton-proton distances and statistical analysis of proton-proton distances in single crystal protein conformations. J. Mol. Biol. 155:321–346, 1982.

24. Wüthrich, K., Billeter, M., Braun, W. Polypeptide secondary structure determination by nuclear magnetic resonance observation of short proton-proton distances. J. Mol. Biol. 180:715–740, 1984.

25. Wüthrich, K., Billeter, M., Braun, W. Pseudo-structures for the 20 common amino acids for use in studies of protein conformations by measurements of intramolecular proton-proton distance constraints with nuclear magnetic resonance. J. Mol. Biol. 180:949–961, 1983.

26. Güntert, P., Braun, W., Billeter, M., Wüthrich, K. Automated stereospecific $^1$H-NMR assignments and their impact on the precision of protein structure determinations in solution. J. Am. Chem. Soc. 111:3997–4004, 1989.

27. Wüthrich, K. "NMR of Proteins and Nucleic Acids." New York: Wiley, 1986.

28. Braun, W., Gō, N. Calculation of protein conformations by proton-proton distance constraints. A new efficient algorithm. J. Mol. Biol. 186:611–626, 1985.

29. Williamson, M.P., Havel, T.F., Wüthrich, K. Solution conformation of the proteinase inhibitor IIA from bull seminal plasma by $^1$H nuclear magnetic resonance and distance geometry. J. Mol. Biol. 182:295–315, 1985.

30. Singh, U.C., Weiner, P.K., Caldwell, J.W., Kollman, P.A., AMBER 3.0, San Francisco: University of California, 1986.

31. Weiner, S.J., Killman, P.A., Nguyen, D.T., Case, D.A. An all atom force field for simulations of proteins and nucleic acids. J. Comp. Chem. 7:230–252, 1986.

32. Billeter, M., Schaumann, Th., Braun, W., Wüthrich, K. Restrained energy refinement with two different algorithms and force fields of the structures of the α-amylase inhibitor Tendamistat determined by NMR in solution. Biopolymers (in press).

33. Billeter, M., Engeli, M., Wüthrich, K. Interactive program for investigation of protein structures based on $^1$H NMR experiments. Mol. Graphics 3:79–83, 97–98, 1985.

34. Eggleston, D.S., Hodgson, D.J. Intramolecular water bridge and a distorted *trans* peptide bond in the crystal structure of α-L-glutamyl-L-aspartic acid hydrate. Int. J. Pept. Protein Res. 26:509–517, 1985.

35. McLachlan, A.D. Gene duplications in the structural evolution of chymotrypsin. J. Mol. Biol. 128:49–79, 1979.

36. Wagner, G., Pardi, A., Wüthrich, K. Hydrogen bond length and $^1$H NMR chemical shifts in proteins. J. Am. Chem. Soc. 105:5948–5949, 1983.

37. Kumar, N.V., Pease, J.H.B., Schweitz, H., Wemmer, D.E. Solution Structure of sea anemone toxins by NMR. ACS Symp. Ser. (in press).

38. Richmond, T.J. Solvent accessible surface area and excluded volume in proteins. J. Mol. Biol. 178:63–89, 1984.

ation networks in biological macromolecules. Biochem. Biophys. Res. Commun. 95:1–6, 1980.